Inorganic Chemistry
Forum Article

Oxygen Isotope Effects as Structural and Mechanistic Probes in Inorganic Oxidation Chemistry

Daniel C. Ashley, David W. Brinkley, and Justine P. Roth*

Department of Chemistry, Johns Hopkins University, 3400 North Charles Street, Baltimore, Maryland 21218

Oxidative transformations using molecular oxygen are widespread in nature but remain a major challenge in chemical synthesis. Limited mechanistic understanding presents the main obstacle to exploiting O_2 in "bioinspired" industrial processes. Isotopic methods are presently being applied to characterize reactions of *natural abundance* O_2 including its coordination to reduced transition metals and cleavage of the $O-O$ bond. This review describes the application of competitive oxygen-18 isotope effects, together with Density Functional Theory, to examine O_2 reductive activation under catalytically relevant conditions. The approach should be generally useful for probing small-molecule activation by transition-metal complexes.

1. Introduction

The activation of a small molecule at a transition-metal center[1,2] is a critical step in numerous biological processes that maintain the world's energy reserves, from the oxidation of water during photosynthesis $(2H_2O \rightarrow O_2 + 4H^+ + 4e^-)$ to the fixation of atmospheric nitrogen $(N_2 + 6H^+ + 6e^- \rightarrow 2NH_3)$. Also included is the subject of this *Inorganic Chemistry* Forum, the reduction and activation of molecular oxygen. Electron transfer to O_2 controls energy balance within the cell during aerobic respiration, biosynthetic reactions, and catabolic processes. Although thermodynamically less challenging than the other examples of small-molecule activation, the selective utilization of oxygen atom equivalents from O_2 is kinetically demanding, often employing multiple metal ions, organic cofactors, and exogenous reductants.

The "reductive activation" of molecular oxygen typically refers to its coordination by a metal complex. Bond formation concomitant with electron transfer results in a metal$-O_2$ adduct, where the oxygen is formally reduced to the level of superoxide (O_2^{I-}) or peroxide (O_2^{II-}). Such species are often weakly basic[3] and/or nucleophilic.[4] Protonation resulting in metal hydroperoxide structures can engender electrophili-

city and give rise to oxidants, as proposed in some heme enzymes.[5,6]

Though metalloproteins use an array of strategies to effect oxidations of strong chemical bonds using O_2, the analogous transformations appear to be more difficult for inorganic compounds in solution. Delineating intrinsic influences from thermodynamic influences upon reaction barriers is essential to progress in this area and the future development of bioinspired catalysts. New experimental approaches are needed to identify metal-activated oxygen intermediates and their mechanisms under catalytically relevant conditions.

This review focuses on the competitive isotope fractionation of *natural abundance* oxygen as a probe of metal-mediated O_2 reactivity in biological and chemical environments. Although the competitive isotope effect has long been appreciated in physical chemistry,[7-10] the technique is more commonly employed as an analytical tool in the food,[11] environmental,[12] and geological sciences.[13,14] There has been

---

*To whom correspondence should be addressed. E-mail: jproth@jhu.edu.

(1) *Activation of Small Molecules: Organometallic and Bioinorganic Perspectives*; Tolman, W. B., Ed.; Wiley: New York, 2006.

(2) Ivanovic-Burmazovic, I.; van Eldik, R. *Dalton Trans.* **2008**, *39*, 5259–5275.

(3) Szajna-Fuller, E.; Bakac, A. *Inorg. Chem.* **2007**, *46*, 10907–10912.

(4) *Active Oxygen in Chemistry*; Foote, C. S., Valentine, J. S., Greenberg, A., Liebman, J. F., Eds.; Chapman & Hall: London, 1995.

(5) Davydov, R.; Chemerisov, S.; Werst, D. E.; Rajh, T.; Matsui, T.; Ikeda-Saito, M.; Hoffman, B. M. *J. Am. Chem. Soc.* **2004**, *126*, 15960–15961.

(6) Newcomb, M.; Aebisher, D.; Shen, R.; Chandrasena, R. E. P.; Hollenberg, P. F.; Coon, M. J. *J. Am. Chem. Soc.* **2003**, *125*, 6064–6065.

(7) Bigeleisen, J. In *Isotopes in Chemistry and Biology*; Kohen, A., Limbach, H.-H., Eds.; CRC Press: Boca Raton, FL, 2006; pp 88−117.

(8) McKinney, C. R.; McCrea, J. M.; Epstein, S.; Allen, H. A.; Urey, H. C. *Rev. Sci. Instrum.* **1950**, *21*, 724–730.

(9) Dole, M.; Rudd, D. P.; Muchow, G. R.; Comte, C. *J. Chem. Phys.* **1952**, *20*, 961–968.

(10) Cahill, A. E.; Taube, H. *J. Am. Chem. Soc.* **1952**, *74*, 2312–2318.

(11) Asche, S.; Michaud, A. L.; Brenna, J. T. *Curr. Org. Chem.* **2003**, *7*, 1527–1543.

(12) Hofstetter, T. B.; Neumann, A.; Arnold, W. A.; Hartenbach, A. E.; Bolotin, J.; Cramer, C. J.; Schwarzenbach, R. P. *Environ. Sci. Technol.* **2008**, *42*, 1997–2003.

(13) Richet, P.; Bottinga, Y.; Javoy, M. *Annu. Rev. Earth Plan. Sci.* **1977**, *5*, 65–110.

(14) Thiemens, M. H. *Annu. Rev. Earth Plan. Sci.* **2006**, *34*, 217–262.

a resurgence of interest in heavy-atom isotope effect measurements, however, because of their utility in comparing reactions of enzymes to those of structurally defined, biomimetic compounds. The measurements also complement theoretical calculations of structure and mechanism. Such combined experimental/computational approaches are increasingly being applied to study transition-metal-mediated small-molecule activation.

Measurements on reactions of O_2 provide unprecedented insights when interpreted using the appropriate level of theory.[15-18] The derived oxygen isotopic effects have been used to (i) differentiate inner-sphere from outer-sphere electron transfer,[19-21] (ii) identify metal$-O_2$ intermediates,[22] and (iii) assess mechanisms of O$-$O bond-breaking/making reactions.[23] Implementing density functional theory (DFT) calibrated for the determination of relevant vibrational frequencies has expanded the scope of structures and mechanisms that can be explored.

2. Competitive Isotope Fractionation

The apparatus and methodology used to measure oxygen kinetic isotope effects (^{18}O KIEs) and equilibrium isotope effects (^{18}O EIEs) on reactions that consume or produce O_2 have been described elsewhere.[15,16,24] A brief outline is provided below to give a sense of the problems that can be addressed using this natural abundance, competitive oxygen isotope fractionation technique. The basic approach to determining ^{18}O KIEs and ^{18}O EIEs, defined according to eqs 1 and 2, involves the creation of an intermolecular competition between $^{16}O^{16}O$ and $^{16}O^{18}O$. ^{18}O in air is only $\sim$0.20%, making the reaction of $^{18}O^{18}O$ negligible. Determining the $^{16}O^{16}O$ versus $^{18}O^{18}O$ effect requires the use of ^{18}O-enriched materials[25] and an appropriately calibrated stable isotope mass spectrometer. ^{17}O enrichment of O_2 has also been employed in competitive experiments aiming to detect magnetic isotope effects,[26] which have been proposed to account for deviations from the normal mass-dependent values.[14]

$$^{18}O \text{ KIE} = \frac{k(^{16}O^{16}O)}{k(^{16}O^{18}O)} \quad (1)$$

$$^{18}O \text{ EIE} = \frac{K(^{16}O^{16}O)}{K(^{16}O^{18}O)} \quad (2)$$

(15) Roth, J. P.; Klinman, J. P. In *Isotope Effects in Chemistry and Biology*; Kohen, A., Limbach, H.-H., Eds.; CRC Press: Boca Raton, FL, 2006; pp 645−669.
(16) Smirnov, V. V.; Brinkley, D. W.; Lanci, M. P.; Karlin, K. D.; Roth, J. P. *J. Mol. Catal. A* **2006**, *251*, 100−107.
(17) Roth, J. P. *Curr. Opin. Chem. Biol.* **2007**, *11*, 142–150.
(18) Roth, J. P. *Acc. Chem. Res.* **2009**, *42*, 399–408.
(19) Mukherjee, A.; Smirnov, V. V.; Lanci, M. P.; Brown, D. E.; Shepard, E. M.; Dooley, D. M.; Roth, J. P. *J. Am. Chem. Soc.* **2008**, *130*, 9459–9473.
(20) Smirnov, V. V.; Roth, J. P. *J. Am. Chem. Soc.* **2006**, *128*, 16424–16425.
(21) Smirnov, V. V.; Roth, J. P. *J. Am. Chem. Soc.* **2006**, *128*, 3683–3695.
(22) Mukherjee, A.; Brinkley, D. W.; Chang, K.-M.; Roth, J. P. *Biochemistry* **2007**, *46*, 3975–3989.
(23) Roth, J. P.; Cramer, C. J. *J. Am. Chem. Soc.* **2008**, *130*, 7802–7803.
(24) Tian, G.; Klinman, J. P. *J. Am. Chem. Soc.* **1993**, *115*, 8891–8897.
(25) Burger, R. M.; Tian, G.; Drlica, K. *J. Am. Chem. Soc.* **1995**, *117*, 1167–1168.
(26) Glickman, M. H.; Cliff, S.; Thiemens, M.; Klinman, J. P. *J. Am. Chem. Soc.* **1997**, *119*, 11357–11361.

The precision of ^{18}O KIE and ^{18}O EIE measurements is limited by systematic errors in the preparation of samples rather than the analytical technique. Isotope ratio mass spectrometry (IRMS) typically gives the $^{18}O/^{16}O$ accurate to $\pm$0.0001−0.0002 or $\pm$0.1−0.2 per mil (‰). Errors are larger in laboratory experiments employing vacuum-line manipulations ($\pm$0.0005−0.0015) but still significantly smaller than the isotope effects themselves, thus allowing for physical interpretations.[16]

The manipulations required to prepare samples for oxygen ($^{18}O/^{16}O$) isotope effect measurements are outlined below. Following the removal of a fixed volume of the reaction solution using a high-vacuum apparatus, O_2 is displaced from the solution by sparging with helium and then passed through a series of cold traps for purification. The O_2 seeded in the helium carrier gas, free of condensables such as CO_2 and water vapor, is quantitatively collected in a liquid N_2-cooled trap containing 5 Å molecular sieves. Following the removal of helium, O_2 is recovered from the molecular sieves by heating.

O_2 is typically combusted to CO_2 for ease of sample handling prior to IRMS analysis.[16] Conversion is achieved in a recirculating furnace equipped with a graphite rod wrapped in platinum wire and heated to $\sim$1100 K. The combustion proceeds in quantitative yield to afford CO_2 with the same $^{18}O/^{16}O$ composition as the O_2. The pressure of CO_2 is precisely determined, and then the gas is transferred into a dry glass tube that is flame-sealed for later analysis by IRMS. Independent experiments are performed to confirm the amount of O_2 consumed or produced following the addition of the reactant to a gas-saturated solution. This quantity is directly related to the ratio of CO_2 pressures before and after a reaction and used to calculate the isotope effect.

IRMS analysis of the CO_2 samples is used to monitor oxygen isotope composition as a reaction progresses. Conversions are typically from 0 to 50%. The $^{18}O/^{16}O$ is determined for each sample versus an internal standard, and the ratio is reported relative to standard mean ocean water (SMOW). The error in the isotope ratio is derived from measurements on unfractionated O_2 performed on the same day in duplicate or triplicate.

A. Competitive ^{18}O KIEs. Methods and Analysis. The ^{18}O KIE can be determined on a reaction that is either stoichiometric or catalytic. A major requirement is that all O_2 remains in solution rather than partitioning into the headspace of the reaction chamber. Experiments in aqueous solutions are therefore conducted with a glass chamber sealed by a movable piston,[15] and experiments in organic solvents are conducted using a solvent-impervious, collapsible bag.[16,41] Both reaction vessels are equipped with injection ports, through which a solution can be introduced to initiate the reaction. An additional requirement is that the amount of O_2 consumed can be precisely determined along with the change in the $^{18}O/^{16}O$.

The precision of the competitively determined ^{18}O KIE on reactions of $^{16}O^{16}O$ and $^{16}O^{18}O$ comes from its formulation in terms of a ratio of isotopic ratios (R_f/R_0) according to eq 3. Multiple measurements are performed to determine R_0, the initial $^{18}O/^{16}O$ in the unreacted O_2, as well as the pressure corresponding to the O_2 concentration in solution. R_f is the $^{18}O/^{16}O$ of the O_2 that remains in solution following a reaction. The $1 - f$ term is

extracted from molar ratios, with f representing the fractional conversion of O_2.

$$^{18}O \text{ KIE} = \left[1 + \frac{\ln(R_f/R_0)}{\ln(1-f)}\right]^{-1} \quad (3)$$

^{18}O KIEs can be determined on reactions where O_2 is consumed or produced from $O_2^{\bullet-}$, H_2O_2, or H_2O. According to eq 4, the isotopic composition of the reactant, defined as R_f, is related to that of the product, R_p, when no other forms of oxygen are present. This relationship has been used to determine ^{18}O KIEs on reactions of superoxide, which was stable in solution on the time scale of the experiments.[20,21]

$$R_0 = R_f(f) + R_p(1-f) \quad (4)$$

A key advantage of the competitive ^{18}O KIE is its precision. The small errors are conservatively reported as 1 standard deviation about the mean rather than the error in the nonlinear curve fitted data. This precision allows for measurements in the presence of small quantities of tracer molecules. Though most stable isotope mass spectrometers are not tuned for the analysis of enriched materials, careful calibration over the prescribed range can be used to determine the effect of adding ^{18}O-enriched O_2, H_2O_2, or H_2O to a reaction with a characteristic isotope fractionation pattern.[23,27] Such experiments have been used to probe reaction reversibility via isotope exchange.[23]

Interpretation of ^{18}O KIEs. The first ^{18}O KIEs on reactions of isolated metalloenzymes with O_2 were measured more than half a century ago by Feldman et al.[28] At the time, little was known about the structures of enzyme active sites and, as a result, the significance of the findings concentrated on the observation that living organisms were capable of fractionating oxygen isotopes in the atmosphere, causing the $^{18}O/^{16}O$ to differ from that of ocean water. Later measurements from the plant biology community suggested that oxygen isotope fractionation patterns could be characteristic of O_2 reduction by the RuBisCo enzymes.[29] Although the foundation for using heavy-atom isotope effects had been in place for some time,[30] it was not until the early 1990s that attempts were made to associate ^{18}O KIEs with the distinct mechanisms used by enzymes that reductively activate O_2.[31]

The use of structurally defined inorganic molecules that undergo defined reactions has led to important progress in understanding the physical origins of ^{18}O KIEs. With regard to O_2 reductive activation, the competitive ^{18}O KIE is comprised of all steps beginning with O_2 encounter and leading up to and including the first irreversible step. It follows that the competitive ^{18}O KIE reflects the ratio of bimolecular rate constants for reactions of O_2 (k_{O_2}), eq 1.

In cases where k_{O_2} encompasses multiple microscopic rate constants, more than one step along the reaction

pathway can be isotopically sensitive and, therefore, contribute to the competitive ^{18}O KIE. Consider the two-step reactions proposed to result in the formation of metal$-O_2$ adducts. Outer-sphere electron transfer from the metal to O_2 in a preequilibrium step is shown in eq 5, where formation of the oxidized metal and $O_2^{\bullet-}$ occurs rapidly prior to combination of the oppositely charged species in the first irreversible step. This mechanism has been the subject of debate in certain O_2-activating metalloenzymes[17,32] including the copper-containing amine oxidases.[19,33,34] A different type of sequential electron transfer is depicted in eq 6, where O_2 binds reversibly, forming an η^1-superoxide complex before rate-limiting reorganization to the η^2-peroxide product. In both cases, the observed ^{18}O KIE is the product of an ^{18}O EIE on the rapid preequilibrium and an ^{18}O KIE on the first irreversible step.

$$(5)$$

$$(6)$$
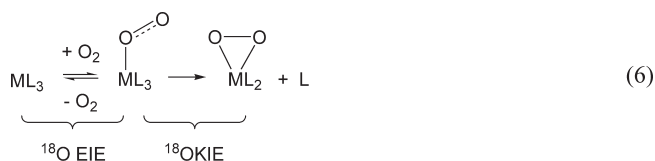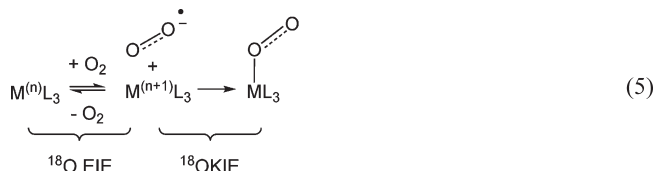
By virtue of being a competitive measurement, the ^{18}O KIE is less obscured by kinetic complexity than an isotope effect derived from absolute rate measurements. In eq 7, for example, the ^{18}O KIE reflects capture of the reactive species in a single, kinetically irreversible step. Thus, information about O_2 reductive activation can be obtained that would otherwise be obscured by ligand dissociation in a noncompetitive measurement. Moreover, the determination of heavy-atom kinetic isotope effects on the basis of absolute rates is exceedingly difficult. Such analyses have been reported for experiments with $^{16,16}O_2$ and $^{18,18}O_2$ as well as $^{14,14}N_2$ and $^{15,15}N_2$.[35,36] In these instances, the size of the isotope effect is comparable to the limits of error.

$$(7)$$
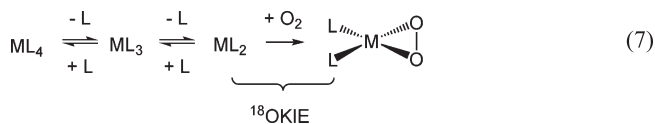
B. Competitive ^{18}O EIEs. Methods and Analysis. The ^{18}O EIE is defined in terms of the equilibrium constants

(27) Chen, H.; Tagore, R.; Olack, G.; Vrettos, J. S.; Weng, T.; Penner-Hahn, J.; Crabtree, R. H.; Brudvig, G. W. *Inorg. Chem.* **2007**, *46*, 34–43.

(28) Feldman, D. E.; Yost, H. T., Jr.; Bensen, B. B. *Science* **1959**, *129*, 146–147.

(29) Helman, Y.; Barkan, E.; Eisenstadt, D.; Luz, B.; Kaplan, A. *Plant Physiol.* **2005**, *138*, 2292–2298.

(30) Melander, L. C.; Saunders, W. H. *Reaction Rates of Isotopic Molecules*; Wiley: New York, 1980.

(31) Tian, G.; Berry, J. A.; Klinman, J. P. *Biochemistry* **1994**, *33*, 226–234.

(32) Purdy, M. M.; Koo, L. S.; Ortiz de Montellano, P. R.; Klinman, J. P. *Biochemistry* **2006**, *45*, 15793–15806.

(33) Mills, S. A.; Goto, Y.; Su, Q.; Plastino, J.; Klinman, J. P. *Biochemistry* **2002**, *41*, 10577–10584.

(34) Shepard, E. M.; Okonski, K. M.; Dooley, D. M. *Biochemistry* **2008**, *47*, 13907–13920.

(35) Palmer, A. E.; Lee, S. K.; Solomon, E. I. *J. Am. Chem. Soc.* **2001**, *123*, 6591–6599.

(36) Laplaza, C. E.; Johnson, M. J. A.; Peters, J.; Odom, A. L.; Kim, E.; Cummins, C. C.; George, G. N.; Pickering, I. J. *J. Am. Chem. Soc.* **1996**, *118*, 8623–8638.

for the reversible binding of $^{16}O^{16}O$ and $^{16}O^{18}O$ (eq 2). It can be determined using the same apparatus as that designed for ^{18}O KIE measurements with slight modification.[15,16,24] Instead of a closed system, an open reaction chamber is employed to allow rapid equilibration of O_2 dissolved in solution and O_2 in the atmosphere.

The addition of a reduced carrier causes uptake such that the total concentration of O_2 increases, $[O_2]^{total} = [O_2]^{bound} + [O_2]^{unbound}$, and exceeds that defined by the solubility of the freely dissolved gas in solution i.e. $[O_2]^{unbound}$. It follows that the measurement of the ^{18}O EIE relies on both the pressure and the isotope composition of O_2 engaged in covalent interaction with a metal, i.e. O_2^{bound}.

The ^{18}O EIE is derived by analyzing the isotope ratio of O_2^{total} (R_t) upon collection of all O_2 from a preequilibrated solution. Thus, the carrier molecule must readily release O_2 when placed under vacuum. R_t is corrected for the isotope ratio of the freely dissolved $O_2^{unbound}$ (R_u) measured independently in the absence of the carrier molecule. The ^{18}O EIE is straightforwardly calculated from R_u/R_t and f, defined here as the fraction of unbound O_2 divided by the total O_2, using eq 8.
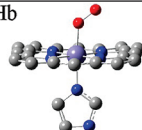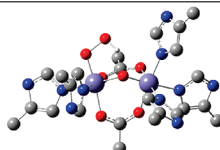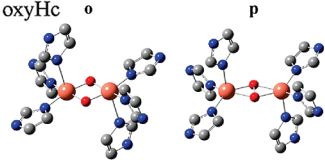
$$^{18}O\ EIE = \frac{1-f}{(R_t/R_u)-f} \qquad (8)$$

Interpretation of ^{18}O EIEs. Klinman and co-workers were the first to determine ^{18}O EIEs on the reversible binding of O_2 to metalloproteins and formation of the oxygenated species in Table 1.[24,37] These reactions involved reductive activation of O_2 by Fe^{II} protoporphyrin IX in hemoglobin (Hb) and myoglobin (Mb), a single Fe^{II} in the bridged diiron site of hemerythrin (Hr), and two neighboring Cu^I sites in hemocyanin (Hc).

The results from this early study were interpreted by considering the bond order change at oxygen. The analysis was based upon the assumption that force constant change is the primary determinant of the ^{18}O EIE.[38] To make the problem tractable, coordination of O_2 to a reduced metal was likened to the addition of an electron and a proton. It was, therefore, reasoned that the ^{18}O EIE upon $Fe(\eta^1$-$O_2)Mb$ formation should resemble the ^{18}O EIE = 1.010 computed for $O_2 + e^- + H^+ \rightleftharpoons HO_2^{\bullet}$, where reduction of the oxygen bond order upon the addition of the electron is partially offset by protonation.

The ^{18}O EIE on $HO_2^{\bullet}$ formation was calculated from the reactant and product vibrational frequencies per the well-known formalism of Bigeleisen and Goeppert-Mayer[39] described in earlier works.[18,24,42,44] While intuitive, the treatment of a reduced metal as a $H^{\bullet}$ equivalent

Table 1. Measured and Calculated ^{18}O EIEs on Reversible O_2 Binding to Metalloproteins

Model	^{18}O EIE$_{exp}$ [a]	^{18}O EIE$_{calc}$ [b]
oxyMb, oxyHb	1.0039(2)– 1.0054(6)	1.0000– 1.0046 [c]
oxyHr	1.0113(5)	1.0115 [d]
oxyHc o p	1.0184(23)	o: 1.0200 [e,g] p: 1.0284 [f,g]

[a] Experimental data are from ref 24. [b] *Gaussian03* calculations performed as outlined in ref 46. [c] The range is for unrestricted singlet-to-triplet states. [d] Computed for an antiferromagnetically coupled low-spin state in refs 18 and 23. [e] **o** = hypothetical bis(μ-oxo) structure. [f] **p** = experimental side-on peroxo structure. [g] The results are identical for the restricted and unrestricted singlet states.

neglects the isotope sensitivity of metal—O bonds as well as the entropic isotope effect associated with losing mass-dependent rotations and translations upon coordinating O_2 to a much heavier metal fragment.

"Cut-off" models[40] based on truncated molecular structures consisting of three atoms and three vibrational modes have been used to more accurately define the ^{18}O EIEs than the metal/$H^{\bullet}$ analogy. Experimental vibrational frequencies corresponding to the isotopic O—O and metal—O bonds can give reasonable results when applied in this way.[41] The cut-off approach was utilized in the first studies of O_2 binding to synthetic transition-metal complexes[41,42] where there seemed to be better agreement between measured and calculated ^{18}O EIEs for η^2-peroxide structures than for η^1-superoxide structures.[43] ^{18}O EIE$_{calc}$ values from 1.026 to 1.031 were calculated for structurally defined, late-transition-metal η^2-peroxide complexes. Using the same cut-off approximation, the ^{18}O EIE$_{calc}$ for η^1-superoxide structures was on average found to be smaller, ranging from 1.011–1.017.[21,43,44] The cut-off approximation appears to inflate ^{18}O EIEs such that the predicted values differ from experimental observations.[21,44]

In a recent study, the cut-off approach was used to compute the ^{18}O EIE for a $Cu^{II}(\eta^1$-OOH) structure in an enzyme active site.[45] A comparison to $Fe^{III}(\eta^1$-OOH) in oxyHr in Table 1[24] suggests that the ^{18}O EIE$_{calc}$ = 1.0258 may be overestimated by a factor of 2. The discrepancy is supported by DFT calculations on $Cu^{II}(\eta^1$-OOH)(L)$_3$ where L = imidazole or methylimidazole, and the ^{18}O EIE$_{calc}$ varies from 1.011 to 1.014.[19] In general, the use of energy-minimized structures together with all vibrational frequencies associated with the molecule gives a more

(37) Isotopic measurements on the irreversible binding of O_2 to dicopper proteins structurally similar to hemocyanin were reported many years earlier in ref 28.

(38) Stern, M. J.; Wolfsberg, M. *J. Chem. Phys.* **1966**, *45*, 2618–2630.

(39) Bigeleisen, J.; Goeppert-Mayer, M. *J. Chem. Phys.* **1947**, *15*, 261–267.

(40) Stern, M. J.; Wolfsberg, M. *J. Phys. Chem.* **1966**, *45*, 4105.

(41) Lanci, M. P.; Brinkley, D. W.; Stone, K. L.; Smirnov, V. V.; Roth, J. P. *Angew. Chem., Int. Ed.* **2005**, *44*, 7273–7276.

(42) Smirnov, V. V.; Lanci, M. P.; Roth, J. P. *J. Phys. Chem. A* **2009**, *113*, 1934–1945.

(43) Lanci, M. P.; Roth, J. P. *J. Am. Chem. Soc.* **2006**, *128*, 16006–16007.

(44) Lanci, M. P.; Smirnov, V. V.; Cramer, C. J.; Gauchenova, E. V.; Sundermeyer, J.; Roth, J. P. *J. Am. Chem. Soc.* **2007**, *129*, 14697–14709.

(45) Only the ν(O—O) and symmetric ν(Cu—O) were used in the analysis: Humphreys, K. J.; Mirica, L. M.; Wang, Y.; Klinman, J. P. *J. Am. Chem. Soc.* **2009**, *131*, 4657–4663.

realistic estimate of the oxygen isotope effect on O_2 reductive activation than the cut-off model.

Applications of DFT to computing structures and the accompanying vibrational frequencies have superseded the use of cut-off models in predicting ^{18}O EIEs. The DFT approach more reliably reproduces not only experimental ^{18}O EIEs on reversible O_2 binding to transition metals but also the temperature dependence of these effects.[42] Using the DFT-based method, we have calculated ^{18}O EIEs for the oxygenated metalloprotein models in Table 1.[46]

In two out of the three structures, calculated and measured ^{18}O EIEs agree well. The exception is oxyHc, a molecule that may present a unique challenge because O_2 is covalently bound between two copper centers. Incidentally, this is one case in which the efficiency of O_2 release was undetermined.[24] Errors in the ^{18}O EIE_{exp} can arise when measurements are performed on solutions that are not completely equilibrated and/ or O_2 is not completely recovered from the metal−O_2 complex.

Several calculations were performed on μ-η^2,η^2-peroxo and bis(μ-oxo) structures as models for oxyHc. Previously published starting geometries with three imidazole ligands to each copper[47] were used and reoptimized with the prescribed DFT method.[46] Calculations on the restricted and unrestricted (broken symmetry) singlet states gave indistinguishable results for the μ-η^2,η^2-peroxo structure, where $d(Cu_1\text{---}Cu_2) = 3.74$ Å and $d(O-O) = 1.43$ Å, as well as the bis(μ-oxo) structure, where $d(Cu_1\text{---}Cu_2) = 2.84$ Å and $d(O\text{---}O) = 2.30$ Å. Starting from coordination geometries with two or three ligands to each copper and changing imidazole to methylimidazole did not alter the results.[48]

OxyHc from various sources has been characterized[49] as a μ-η^2,η^2-peroxide bonded to two antiferromagnetically coupled, tricoordinate Cu^{II} centers.[50] Although the DFT calculations reproduce the metrical data and electronic ground state, the ^{18}O $EIE_{calc} = 1.0284$ from full-frequency analysis is significantly larger than the reported ^{18}O $EIE_{calc} = 1.0184(23)$. Interestingly, the μ-oxo structure is computed to have a smaller ^{18}O $EIE_{calc} = 1.0200$, closer to the experimental value.

As mentioned above, oxyHc is the only structure examined where O_2 is activated by bonding to two transition-metal centers. It is possible that the DFT calculations underestimate the number of isotopically sensitive, low-frequency modes in this case. Including additional isotopic modes in the calculations would cause the ^{18}O EIE to decrease because of an increased isotope shift of vibrations within the oxygenated product relative to O_2.

3. Theoretical Basis of ^{18}O EIEs

The formalism of Bigeleisen and Goeppert-Mayer[39] is commonly used to compute ^{18}O EIEs. The fundamental equation is derived for an isotope exchange reaction in the gas phase, i.e., eq 9, where the asterisk designates the site of the heavy isotope. The isotope exchange is the difference of two equilibria, $M + O_2 \rightleftharpoons MO_2$ and $M + O_2^* \rightleftharpoons MO_2^*$, and results in the ratio of equilibrium constants given above in eq 2.

$$O_2^* + M-O_2 \rightleftharpoons O_2 + M-O_2^* \tag{9}$$
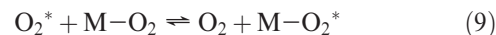
The ^{18}O EIE is computed for isotope exchange in terms of reduced gas-phase partition functions (eq 10). Terms include the zero-point energy (ZPE), the energy of excited vibrational states (EXC), and the mass and moments of inertia (MMI). Each partition function invokes all vibrational frequencies of the isotopologues in the reactant and product states. Alternatively, the mass and moments of inertia can be computed using a classical expression that depends only on molecular masses and rotational constants. We designate this partition function as MMI_{rot} to distinguish it from the one computed from vibrations. Agreement between the MMI and MMI_{rot} establishes the validity of eq 10 as well as the quality of DFT-optimized structures.[51] In general, solvent corrections applied to the DFT-derived structures result in negligible variation of the isotopic partition functions (see below).

$$^{18}O \text{ EIE} = ZPE \times EXC \times MMI \tag{10}$$

ZPE derives from the change in the force constant that occurs upon conversion of the reactant state into the product state. The contribution is dominant for ^{18}O EIEs upon reduction of O_2 in the absence of concomitant bond formation to a metal. A *normal* (>1) isotope effect on the zero point energy level splitting (given in parentheses) arises from weakening of the bonding interactions such that there is a decrease in the molecular force constant. Examples include the conversion of O_2 to $O_2^{\bullet-}$ (1.034) and $HO_2^{\bullet}$ (1.010). The situation is different for O_2 reductive activation by a transition-metal complex. Upon coordination of O_2, the formation of metal−O bonds causes an *inverse* (<1) ZPE as depicted in Figure 1. The overall bonding within the product is strengthened in spite of reducing the O−O bond.[52] Opposite to intuition based on the metal/H$^{\bullet}$ analogy, the increase in the force constant and attendant increase in the zero point energy level splitting ($\triangle$) are consistent with the favorable enthalpies associated with O_2 binding to transition-metal complexes.[43]

The EXC partition function reflects the relative population of vibrational energy levels associated with the light and heavy isotopes. Inverse EXC terms are observed when there is an increase in the number of bonding modes within the product from that in the reactant. The closer spacing of the vibrational energy levels associated with the heavier isotopologue

(46) The following atomic orbital basis functions were used: Ni, Co, Fe, and Cl (the compact relativistic effective core potential basis CEP-31G), Pd and Rh (LANL2DZ), N and O (6-311G*), P (6-311G**), C (6-31G), and H (STO-3G). The stability of the final wave function solution was confirmed for each optimized structure. Molecular geometries were fully optimized using *mPWPW91* as implemented in *Gaussian03*:Frisch, M. J.; et al. *Gaussian03*, revision C.02; Gaussian, Inc.: Pittsburgh, PA, **2003**.

(47) Cramer, C. J.; Wloch, M.; Piecuch, P.; Puzzarini, C.; Gagliardi, L. *J. Phys. Chem. A* **2006**, *110*, 1991–2004.

(48) The μ-η^2,η^2-peroxo structure with three methylimidazole ligands at one copper and two at the other gave ^{18}O $EIE_{calc} = 1.0284$, while a bis(μ-oxo) structure with two methylimidazole ligands at each copper gave ^{18}O $EIE_{calc} = 1.0168$.

(49) Ling, J.; Nestor, L. P.; Czernuszewicz, R. S.; Spiro, T. G.; Fraczkiewicz, R.; Sharma, K. D.; Loehr, T. M.; Sanders-Loehr, J. *J. Am. Chem. Soc.* **1994**, *116*, 7682–7691.

(50) Henson, M. J.; Mahadevan, V.; Stack, T. D. P.; Solomon, E. I. *Inorg. Chem.* **2001**, *40*, 5068–5069.

(51) Wolfsberg, M. In *Isotopes in Chemistry and Biology*; Kohen, A., Limbach, H.-H., Eds.; CRC Press: Boca Raton, FL, 2006; pp 89−117.

(52) In contrast, weakening of the O−O force constant was proposed to be the primary determinant of ^{18}O EIE in refs 24 and 25.
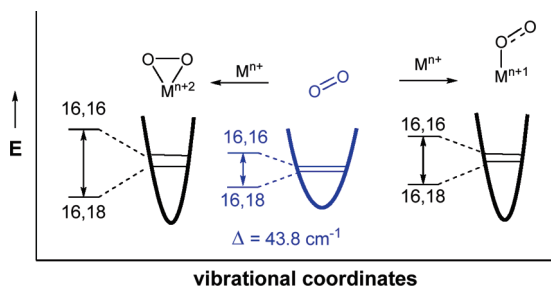
Figure 1. Origin of the inverse ZPE effect upon O_2 binding to a reduced transition metal.

results in a greater population than in the lighter one. A normal EXC would arise in the opposite situation, if product formation were associated with a decrease in bonding modes, as expected when small molecules dissociate from metal complexes.

The MMI represents the isotopic partition function deriving from changes in mass-dependent rotations and translations. This classical effect is temperature-independent and falls within the range of 1.14−1.15 for the competitive binding of ^{16}O ^{16}O versus ^{16}O ^{18}O. The size of MMI makes it the largest contributor among the isotopic partition functions in eq 10. Analyzing the MMI term alone can be misleading, however. When O_2 coordinates to a metal, the molecule's rotational and translational degrees of freedom are converted into new low-frequency bonding modes. It follows that the large normal MMI is partially offset by the inverse EXC.

EXC × MMI is the equivalent of the isotope effect on the reaction entropy, while ZPE is the equivalent of the isotope effect on the reaction enthalpy. The EXC × MMI value is large and normal for all metal-mediated O_2 reductive activations when determined by full-frequency analysis, indicating that this contribution dominates the inverse ZPE at most temperatures. Entropy−enthalpy compensation, as revealed by the changing contributions of the calculated partition functions, leads to a nonlinear temperature dependence of the ^{18}O EIEs and deviations from van't Hoff behavior.[42]

4. DFT in Isotope Effect Calculations

Analysis of the full complement of isotopic vibrations is required to "correctly" apply Bigeleisen and Goeppert-Mayer's formalism. The reason is that eq 10 is defined on the basis of the Redlich−Teller product rule, which relates frequency to mass and allows the reduced partition functions to be expressed exclusively in terms of vibrations.[51]

The vibrations used in the calculations described here are obtained from DFT-derived minimum-energy structures. Each mode of the reactant and product is treated as a harmonic oscillator and its frequency considered without scaling. While the impact of anharmonicity is difficult to assess, it is anticipated that such behavior should be most important for the lowest frequency modes. Yet isotopic vibrational frequencies are typically greater than 200 cm^{-1} for metal−O_2 complexes, resulting in insignificant populations of these modes.

Consistent with the absence of complications due to anharmonicity, ^{18}O EIEs have been calculated to within a few tenths of a percent (±0.0003) and used to discriminate between metal−O_2 complexes of the same structural type. For example, average isotope effects for $Co(\eta^1\text{-}O_2)$

complexes (^{18}O $EIE_{ave} \sim 1.005$) are calculated and observed to be significantly smaller than those for $Cu(\eta^1\text{-}O_2)$ complexes (^{18}O $EIE_{ave} \sim 1.012$). In addition, experiments have corroborated the unique temperature profiles of ^{18}O EIEs predicted for η^1-superoxide and η^2-peroxide complexes (see below).

There appears to be greater uncertainty when analyzing experimentally assigned vibrations within the cut-off model than when making the harmonic approximation in full-frequency analyses. When using the minimum number of three isotopic vibrational frequencies for a metal−O_2 complex, the net isotope shift is often underestimated due to the presence of mode mixing, resulting in an inflated ^{18}O EIE. A discrepancy of a few cm^{-1} ($\sim$8.5 cal mol^{-1}) translates into an error of ±0.0005, which is comparable to the magnitude of some ^{18}O EIEs. The cut-off model is also characterized by anomalies in the reduced partition functions. MMI can be 5 times smaller than MMI_{rot} when the term is calculated from a truncated set of vibrations. It follows that EXC × MMI is minimized by the cut-off model while ZPE is rendered less inverse and sometimes slightly normal. Clearly, the physical meanings are compromised as are the predicted temperature profiles of the ^{18}O EIEs.

The DFT method used for the calculation of oxygen isotope effects was originally optimized by Cramer and co-workers to reproduce isotopic vibrational frequencies of Cu−O_2 complexes.[53] With respect to ^{18}O EIE calculations, the importance of using a local functional (mPWPW91), together with sufficiently large basis sets to describe oxygen and the transition-metal center, has since been demonstrated. In most if not all cases where the optimized protocol has been applied to O_2 activation at a first- or second-row transition-metal center, the ^{18}O EIE_{calc} agrees well with the ^{18}O EIE_{exp}. Treating the solvation of the metal−O_2 complex and O_2 using the polarized continuum model can give slightly better agreement at the expense of significant computing time.[42,44]

The performance of mPWPW91 in calculating ^{18}O EIEs is superior to the more common hybrid functional B3LYP; this is likely because the systems of interest exhibit substantial multiconfigurational character.[54] Yet even for O_2 the performance of B3LYP is poor. When mPWPW91 is applied along with the 6-311G* basis set on oxygen, the O−O stretching frequencies are in good agreement with the experimental results: $^{16,16}\omega_{exp} = 1556.3$ cm^{-1} versus $^{16,16}\omega_{calc} = 1548.9$ and $^{16,18}\Delta_{exp} = -43.8$ cm^{-1} versus $^{16,18}\Delta_{calc} = -43.7$ cm^{-1}.[42] Larger deviations are seen with B3LYP and the 6-31+G* basis ($^{16,16}\omega_{calc} = 1641.2$ cm^{-1} and $^{16,18}\Delta_{calc} = -46.3$ cm^{-1}) as well as BP86 and the TZVP basis ($^{16,16}\omega_{calc} = 1522.5$ cm^{-1} and $^{16,18}\Delta_{calc} = -43.0$ cm^{-1}), both of which have been used to compute ^{18}O EIEs published in the literature.[55,56]

DFT calculations offer better agreement between measured and calculated ^{18}O EIEs than matching of experimental O−O and metal−O stretching frequencies. This point is

(53) Kinsinger, C. R.; Gherman, B. F.; Gagliardi, L.; Cramer, C. J. *J. Biol. Inorg. Chem.* **2005**, *10*, 778–789.

(54) Cramer, C. J.; Gour, J. R.; Kinal, A.; Wloch, M.; Piecuch, P.; Shahi, A.; Rehaman, M.; Gagliardi, L. *J. Phys. Chem. A* **2008**, *112*, 3754–3767.

(55) Popp, B. V.; Wendlandt, J. E.; Landis, C. R.; Stahl, S. S. *Angew. Chem., Int. Ed.* **2007**, *46*, 601–604.

(56) Mirica, L. M.; McCusker, K. P.; Munos, J. W.; Liu, H.; Klinman, J. P. *J. Am. Chem. Soc.* **2008**, *130*, 8122–8123.

illustrated by the simple reaction $O_2 + 2e^- + 2H^+ \rightleftharpoons H_2O_2$. In earlier studies, an ^{18}O $EIE_{calc} = 1.0089$ was extracted from experimental data[57] and H_2O_2 force constants derived from normal mode analysis ($^{16,16}\omega_1 = 3606.4$ cm^{-1}, $^{16,18}\Delta_1 = -0.1$ cm^{-1}, $^{16,16}\omega_2 = 3606.4$ cm^{-1}, $^{16,18}\Delta_2 = -11.3$ cm^{-1}, $^{16,16}\omega_3 = 1396.7$ cm^{-1}, $^{16,18}\Delta_3 = -2.5$ cm^{-1}, $^{16,16}\omega_4 = 1264.9$ cm^{-1}, $^{16,18}\Delta_4 = -2.5$ cm^{-1}, $^{16,16}\omega_5 = 863.3$ cm^{-1}, $^{16,18}\Delta_5 = -24.0$ cm^{-1}, $^{16,16}\omega_6 = 320.2$ cm^{-1}, $^{16,18}\Delta_6 = -0.4$ cm^{-1}).[24] Here the net isotope shift is $\Sigma(^{16,18}\Delta) = -40.8$, resulting in ZPE = 1.0029, EXC = 0.9976, and MMI = 1.008 37. The latter is somewhat smaller than MMI$_{rot}$ = 1.0100 computed independently, suggesting small errors in the normal mode analysis.

There is reasonable agreement with the ^{18}O $EIE_{calc} = 1.0070$ when *m*PWPW91 is used together with 6-311G* on O and STO-3G on H although the vibrational frequencies differ ($^{16,16}\omega_1 = 3432.0$ cm^{-1}, $^{16,18}\Delta_1 = -1.8$ cm^{-1}, $^{16,16}\omega_2 = 3427.8$ cm^{-1}, $^{16,18}\Delta_2 = -9.8$ cm^{-1}, $^{16,16}\omega_3 = 1432.7$ cm^{-1}, $^{16,18}\Delta_3 = -3.3$ cm^{-1}, $^{16,16}\omega_4 = 1283.7$ cm^{-1}, $^{16,18}\Delta_4 = -3.1$ cm^{-1}, $^{16,16}\omega_5 = 899.6$ cm^{-1}, $^{16,18}\Delta_5 = -25.3$ cm^{-1}, $^{16,16}\omega_6 = 319.7$ cm^{-1}, $^{16,18}\Delta_6 = -0.6$ cm^{-1}) along with the net isotope shift $\Sigma(^{16,18}\Delta) = -43.9$, ZPE = 0.9993, EXC = 0.9975, and MMI = 1.0102.

Increasing the size of the basis on H to 6-31G affords better agreement with certain vibrational frequencies and poorer agreement with others: ($^{16,16}\omega_1 = 3613.5$ cm^{-1}, $^{16,18}\Delta_1 = -1.4$ cm^{-1}, $^{16,16}\omega_2 = 3610.3$ cm^{-1}, $^{16,18}\Delta_2 = -10.9$ cm^{-1}, $^{16,16}\omega_3 = 1449.7$ cm^{-1}, $^{16,18}\Delta_3 = -3.3$ cm^{-1}, $^{16,16}\omega_4 = 1288.8$ cm^{-1}, $^{16,18}\Delta_4 = -2.9$ cm^{-1}, $^{16,16}\omega_5 = 900.5$ cm^{-1}, $^{16,18}\Delta_5 = -25.3$ cm^{-1}, $^{16,16}\omega_6 = 325.3$ cm^{-1}, $^{16,18}\Delta_6 = -0.7$). The net isotope shift of $\Sigma(^{16,18}\Delta) = -44.5$, ZPE = 0.9998, EXC = 0.9975, and MMI = 1.0101 results in a decrease in the ^{18}O $EIE_{calc} = 1.0055$.

To probe the sensitivity to the functional and basis sets, we have recalculated the ^{18}O EIE on $O_2 + 2e^- + 2H^+ \rightleftharpoons H_2O_2$ using the other published methods.[55,56] Consistent with the somewhat poorer quality of these calculations, larger deviations from the experimental vibrational frequencies are observed. Using B3LYP together with 6-31+G* gives a net isotope shift of $\Sigma(^{16,18}\Delta) = -44.5$, ZPE = 1.0047, EXC = 0.9976, and MMI = 1.0101 resulting in an ^{18}O $EIE_{calc} = 1.0124$, while using BP86, the TZVP basis on O and 6-31G or 6-31G* on H gives a net isotope shift of $\Sigma(^{16,18}\Delta) = -44.0$, ZPE = 0.9978, EXC = 0.9975, and MMI = 1.0101 resulting in an ^{18}O $EIE_{calc} = 1.0053$.

Lower isotope sensitivity of the modes extracted from experimental data is the cause of the variation in the computed ^{18}O EIEs. All of the DFT calculations using the local functionals indicate a greater isotope shift and an ^{18}O $EIE_{calc} = 1.0053 - 1.0055$, in good agreement with an earlier solution-phase value of 1.0054 estimated by Dole et al.[9] Analysis of the spectroscopic data for H_2O_2 has since employed anharmonic corrections.[58] Although it is tempting to attribute part of the discrepancy in the calculations to anharmonic behavior, this case is not without ambiguity. Experiments have shown the

vibrational frequencies of H_2O_2 to be both matrix- and phase-dependent,[59,60] calling into question some of the force constants from the early studies.

A. Characterization of Metal–O₂ Complexes. Coordination Modes and Formal Oxidation States. The importance of predicting ^{18}O EIEs on the basis of carefully optimized structures and full sets of isotopic vibrational frequencies is clear. The point has been convincingly demonstrated by full-frequency analyses that have reproduced measured ^{18}O EIEs for a variety of η^1-superoxide structures (1.004–1.015) and η^2-peroxide structures (1.020–1.030) as well as their characteristic temperature dependences.[18,42–44] The distinctive ranges are attributed to entropic contributions represented by the EXC × MMI in full-frequency models. Because MMI is ~1.15 for reactions where there is competitive binding of $^{16}O^{16}O$ and $^{16}O^{18}O$, the variation is mostly due to the EXC term, which reflects the different populations of isotopic low-frequency modes. The predictability of the ^{18}O EIEs bodes well for applications that involve identifying reactive intermediates, which cannot be isolated and are often spectroscopically undetectable under catalytic conditions.

^{18}O EIEs intermediate of those associated with η^1-superoxide and η^2-peroxide coordination modes are expected for formally η^1-peroxide or η^2-superoxide structures. This hypothesis is consistent with ^{18}O EIE calculations on a cationic Cr^{III} η^2-superoxide complex with ^{t}Bu,Me-Tp = hydrotris(3-*tert*-butyl-5-methylpyrazolyl)-borate and Pz′H = 3-*tert*-butyl-5-methylpyrazole supporting ligands.[61] Structural and magnetic measurements by Theopold and co-workers indicate strong antiferromagnetic coupling between the d^3 metal ion and $O_2^{\bullet-}$, resulting in a triplet ground state.

The Cr$^{III}(\eta^2$-O_2) species has subsequently been characterized using the DFT protocol outlined above.[46,62] Agreement is observed between crystallographically determined bond lengths and those extracted from the computationally optimized structure: $d(O-O)_{exp} = 1.327(5)$ Å and $d(Cr-O)_{exp}$ 1.861(4)–1.903(4) Å versus $d(O-O)_{calc} = 1.35$ Å and $d(Cr-O)_{calc} = 1.90$ Å. The experimental O–O stretching frequency, $^{16,16}\omega_{exp} = 1072$ cm^{-1} is reproduced reasonably well by the gas-phase calculation. Although coupling to ligand modes obscures the O–O vibration at $^{16,16}\omega_{calc} = 1018.5$ cm^{-1}, the shift upon double isotope substitution is as expected, $^{18,18}\omega_{calc} = 960.6$ cm^{-1}.[46] Binding of O_2 is kinetically irreversible in this system, precluding experimental verification of the ^{18}O $EIE_{calc} = 1.0157$ which falls just outside the ranges associated with η^1-superoxide and η^2-peroxide structures.

Intermediate values of ^{18}O EIEs are also predicted for Cu–O₂ complexes with hybrid electronic structures. Such descriptions have been proposed for Cu(η^2-O_2)^{t}Bu-Tp and Cu(η^2-O_2)(βDK) in Figure 2.[63] In the absence of experimental data, calculations performed on the unstable [Cu(η^1-O_2)TMPA]$^+$ and [Cu(η^1-O_2)TEPA]$^+$ assumed singlet ground states. Spectroscopic resemblance of the former complex to [Cu(η^1-O_2)TMG$_3$tren]$^+$

(57) Giguère, P. A.; Srinivasan, T. K. K. *J. Raman Spectrosc.* **1974**, *2*, 125–132.

(58) Dorofeeva, O. V.; Iorish, V. S.; Novikov, V. P.; Neumann, D. B. *J. Phys. Chem. Ref. Data* **2003**, *32*, 879–894.

(59) Pettersson, M.; Tuominen, S.; Räsänen, M. *J. Phys. Chem. A* **1997**, *101*, 1166–1171.

(60) Rauhut, G.; Knizia, G.; Werner, H.-J. *J. Chem. Phys.* **2009**, *130*, 054105/1–054105/5.

(61) Qin, K.; Incarvito, C. D.; Rheingold, A. L.; Theopold, K. H. *Angew. Chem., Int. Ed.* **2002**, *41*, 2333–2335.

(62) Cramer, C. J.; Tolman, W. B.; Theopold, K. H.; Rheingold, A. L. *Proc. Natl. Acad. Sci. U.S.A.* **2003**, *100*, 3635–3640.

(63) Sarangi, R.; Aboelella, N.; Fujisawa, K.; Tolman, W. B.; Hedman, B.; Hodgson, K. O.; Solomon, E. I. *J. Am. Chem. Soc.* **2006**, *128*, 8286–8296.
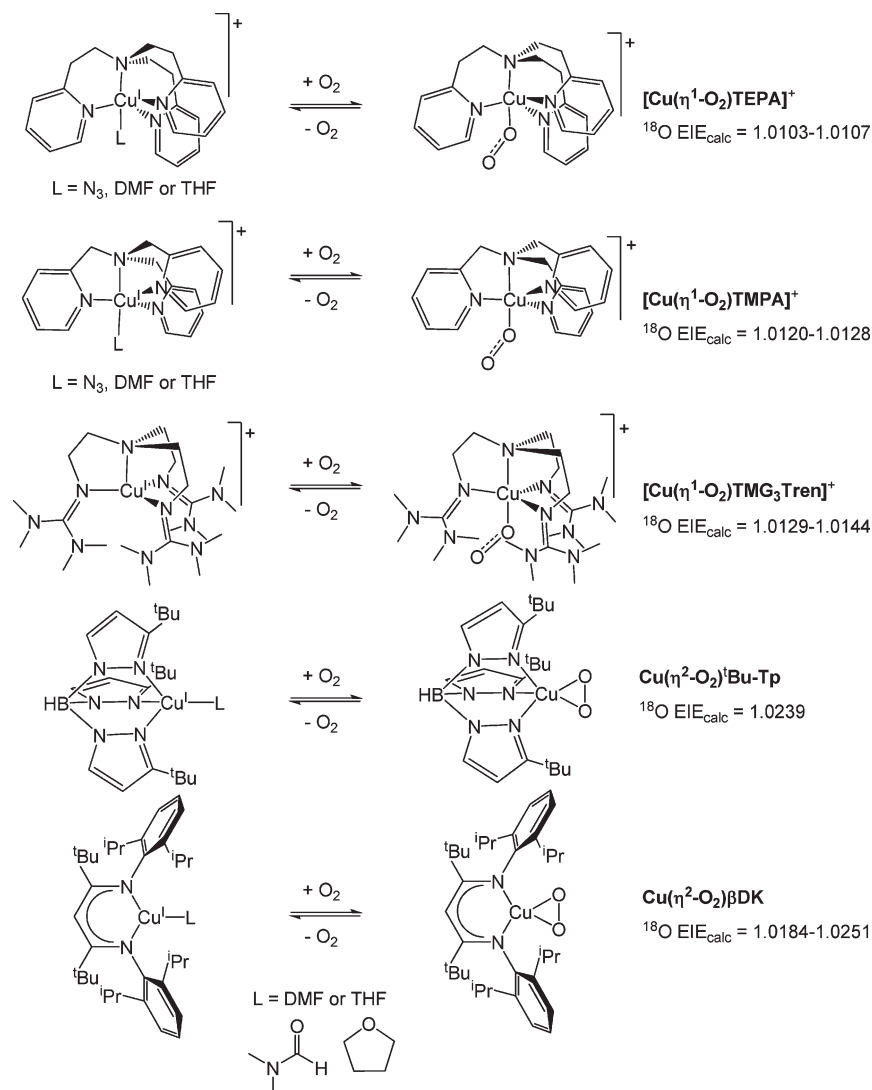
Figure 2. Maximum ^{18}O EIEs on Cu–O$_2$ formation derived from DFT calculations. Ranges are given for the electronic ground states indicated in Table 2 (below).[44]

Table 2. ^{18}O EIEs and Partition Functions for the Reactions in Figure 2[44]

product (spin state)[a]	$T_{max}(K)$[b]	EIE	ZPE	EXC	MMI	MMI$_{rot}$[c]
$[Cu(\eta^1$-O$_2)$TEPA$]^+$ (s)	301	1.0103	0.9572	0.9211	1.1458	1.1460
$[Cu(\eta^1$-O$_2)$TEPA$]^+$ (bs)	243	1.0107	0.9597	0.9192	1.1457	1.1452
$[Cu(\eta^1$-O$_2)$TMPA$]^+$ (s)	266	1.0120	0.9671	0.9167	1.1415	1.1423
$[Cu(\eta^1$-O$_2)$TMPA$]^+$ (bs)	222	1.0128	0.9644	0.9207	1.1406	1.1420
$[Cu(\eta^1$-O$_2)$TMG$_3$tren$]^+$ (s)	255	1.0144	0.9581	0.9214	1.1492	1.1508
$[Cu(\eta^1$-O$_2)$TMG$_3$tren$]^+$ (bs)	247	1.0134	0.9588	0.9182	1.1512	1.1510
$[Cu(\eta^1$-O$_2)$TMG$_3$tren$]^+$ (t)	243	1.0129	0.9589	0.9174	1.1515	1.1509
Cu$(\eta^2$-O$_2)^t$Bu-Tp (bs)	173	1.0239	0.9529	0.9367	1.1472	1.1485
Cu$(\eta^2$-O$_2)\beta$DK (s)	259	1.0184	0.9556	0.9273	1.1493	1.1508
Cu$(\eta^2$-O$_2)\beta$DK (bs)	197	1.0251	0.9558	0.9337	1.1487	1.1507

[a] Calculations were constrained to s = restricted singlet, bs = unrestricted/broken symmetry singlet, and t = triplet spin states. [b] Temperature associated with the maximum ^{18}O EIE computed from vibrational frequencies using eq 10 in ref 44. [c] MMI$_{rot}$ calculated independently from masses and rotational constants.

suggests that a triplet ground state due to ferromagnetic coupling of spins on Cu^{II} and O$_2$$^{\bullet-}$ is also possible.[44]

For the purposes of comparison, ^{18}O EIEs in Figure 2 are given at a characteristic T_{max}, the temperature where the isotope effect is a maximum. Further details are provided in Table 2. The determination of the maximum ^{18}O EIEs and T_{max} required consideration of the partition functions in eq 10. The gas-phase geometries and, consequently, the vibrational frequencies were assumed to be temperature independent. The results reveal that ^{18}O EIEs are largely determined by the O$_2$ coordination mode. Interestingly, there is no trend in the ZPE contribution. Instead, EXC × MMI is the primary determinant of the ^{18}O EIE. The latter entropic isotope
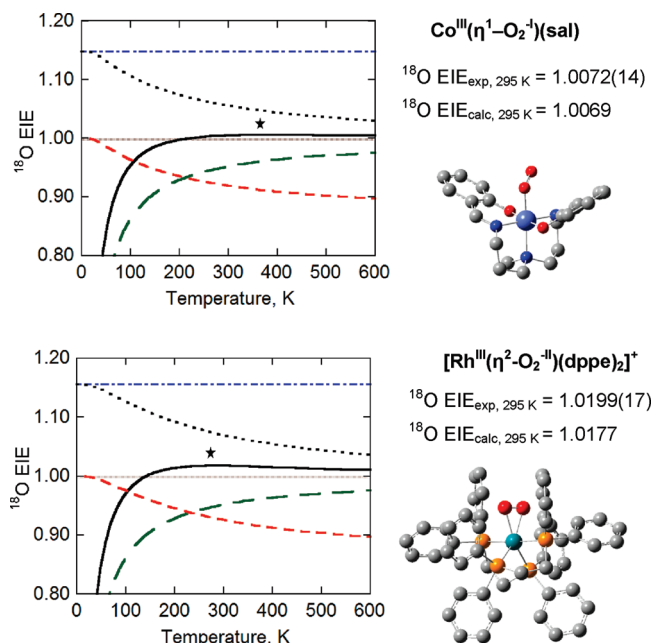
Figure 3. Temperature profiles for O_2 binding to $Co^{II}(sal)$ and $[Rh^I(dppe)_2]Cl$ to form $Co^{III}(\eta^1-O_2)(sal)$ and $[Rh^{III}(\eta^2-O_2)(dppe)_2]Cl$. Full-frequency analysis of gas-phase-optimized structures was used to compute the ^{18}O EIEs (—), ZPE (− −), EXC (- - -), MMI (·-·), EXC × MMI (· · ·), and T_{max} (★).

effect is 1.5−2 times greater for η^2 coordination than for η^1 coordination regardless of the electronic ground state.

The larger ^{18}O EIEs and lower T_{max}'s parallel the stability of the $Cu-O_2$ complexes with respect to O_2 dissociation. In general, the η^2 complexes are thermodynamically stabilized relative to the η^1 complexes because of the additional $Cu-O$ bond, which is formed at the expense of weakening the $O-O$ bond. As discussed in the following section, the enhanced stability is associated with smaller numbers of low-frequency vibrations and larger contributions to the ^{18}O EIE from EXC × MMI.

Temperature Considerations. The temperature dependence of ^{18}O EIEs arises from entropy−enthalpy compensation. This phenomenon, anticipated from the physical description of reduced gas-phase partition functions, is depicted in Figure 3. The predicted temperature profiles for the η^1-superoxide and η^2-peroxide structures are distinguished by variations in the magnitude of the ^{18}O EIE as well as T_{max}, defined above. Experimental studies of oxygenation reactions that give rise to $Co^{III}(\eta^1-O_2)(sal)$ and $[Rh^{III}(\eta^2-O_2)(dppe)_2]^+$, where sal = bis-[3-(salicylideneamino)propylmethylamine] and dppe = 1,2-bis(diphenylphosphino)ethane, have corroborated the theoretical predictions over a range of temperatures.[42] T_{max} is expected to be lower for the η^2-coordination geometry than the η^1-coordination geometry because of differences in the number of isotopic low-frequency vibrational modes.

Basic trends appear to characterize reversible O_2 binding reactions. Similar trends have been observed by Parkin and coworkers for H_2 activation (i.e., the formation of σ-bound complexes) and contrasted to the behavior associated with H_2 oxidative addition

involving reversible cleavage of the $H-H$ bond.[64] ^{18}O EIEs on O_2 reductive activation to the level of superoxide or peroxide begin inverse at the lowest temperature and increase through a normal maximum before decreasing to 1 as the temperature approaches infinity. This is the result of a decrease in the entropic isotope effect (EXC × MMI) and an increase in the enthalpic isotope effect (ZPE).

Understanding the temperature dependence of ^{18}O EIEs requires analysis of the isotopic partition functions. As the temperature increases, EXC approaches the constant 1/MMI term. This effect reflects the changing populations of vibrational energy levels associated with the light and heavy isotopologues. At the limit of infinite temperature, there is no difference in the Boltzmann distributions and EXC × MMI is unity. Starting from the lowest temperature, as EXC × MMI decreases, ZPE becomes less inverse and approaches 1 at the high-temperature limit. When the change in ZPE with temperature dominates the change in EXC × MMI, the ^{18}O EIE increases. This is the origin of the increasing isotope effect observed for the η^1-O_2 complexes.[42] The opposite trend is observed for η^2-O_2 complexes, when the decrease in EXC × MMI dominates the increase in ZPE. The transition from inverse to normal ^{18}O EIE arises from a crossover from a dominant ZPE contribution at low temperatures to a dominant EXC × MMI contribution at higher temperatures.

One additional point concerns the assumptions made when computing temperature dependent ^{18}O EIEs for reactions in solution. Although vibrations are inherently temperature independent, the dielectric constant exhibits variation in a manner unique to the solvent. Thus, changing the temperature can influence solvated structures and indirectly affect the vibrational frequencies of a metal−O_2 adduct. Small deviations between calculated and measured ^{18}O EIEs have been indicated in some cases and reduced by including solvent dielectric corrections in the DFT calculations.[42,44] Agreement with the experimental $O-O$ vibrational frequencies can also be improved to within 80 cm^{-1} when solvation is treated explicitly.

B. ^{18}O EIEs as Boundary Conditions of ^{18}O KIEs. Computational methods have recently been applied in an effort to illuminate the physical relationship between heavy-atom equilibrium isotope effects and the constituent kinetic isotope effects.[18,19,23,42,54,55,65,66] Experimental studies of kinetically irreversible O_2 coordination reactions have indicated that ^{18}O KIEs are less than the corresponding ^{18}O EIEs,[41] although the underlying physical explanation for this behavior is obscure. The reasoning originated from interpretations of ^{18}O KIEs by analogy with secondary isotope effects. The equilibrium isotope effects reflecting bond rehybridization were taken to be upper limits.[15,24] Though the relationship ^{18}O KIE < ^{18}O EIE has been corroborated for single-step O_2 binding, there is no experimental evidence to evaluate the assumption for other types of O_2 reductive activation reactions, most ostensibly those involving $O-O$ bond cleavage.

(64) Janak, K. E.; Parkin, G. *J. Am. Chem. Soc.* **2003**, *125*, 13219−13224.

(65) Ralph, E. C.; Hirschi, J. S.; Anderson, M. A.; Cleland, W. W.; Singleton, D. A.; Fitzpatrick, P. F. *Biochemistry* **2007**, *46*, 7655−7664.

(66) Kelly, K. K.; Hirschi, J. S.; Singleton, D. A. *J. Am. Chem. Soc.* **2009**, *131*, 8382−8383.

Considering an inner-sphere electron transfer to O_2, the magnitude of the ^{18}O KIE is assumed to be influenced by isotopic bond reorganization in the transition state. The Hammond postulate, which envisages the transition state as resembling the structure of the closest energy species, predicts the largest kinetic isotope effect for a product-like transition state in an endothermic reaction. In contrast, Marcus Theory places the maximum isotope effect at $\triangle G° = 0$ kcal mol^{-1}, where the transition state has been described as most symmetric.[30] At this point, the intrinsic contribution to the ^{18}O KIE is unabated by the reaction thermodynamics.[15-17] Experiments to determine ^{18}O KIEs and ^{18}O EIEs over a range of positive and negative $\triangle G°$ values are needed to test the models above. Incidentally, all reactions examined to date reflect O_2 coordination in the thermodynamically favorable direction.

5. Calculating ^{18}O KIEs

The calculation of ^{18}O KIEs is more challenging than the calculation of ^{18}O EIEs because of uncertainty regarding the reaction coordinate and transition-state structure. In addition, ^{18}O KIEs may reflect reactions involving multiple isotopically sensitive microscopic steps. This complication was mentioned above in relation to eqs 5 and 6 and will be elaborated upon in the discussion below.

Though a significant portion of the metal$-O_2$ binding affinity derives from covalent interaction, there are cases where the formation of an unbound superoxide or peroxide intermediate is proposed to occur in a preequilibrium step. Considering outer-sphere electron transfer followed by the rapid combination of $O_2^{•-}$ and oxidized metal species (eq 5), an intermediate might not be detectable. Such a reaction would still exhibit a characteristic ^{18}O KIE.[17,32,33] In some instances, outer-sphere electron-transfer mechanisms can be excluded on the basis of redox potentials, assuming appropriate electrostatic corrections for stabilization of $O_2^{•-}$ by a nearby point charge.[67,68] In cases where the thermodynamics is not prohibitive, the ^{18}O KIE should be the product of the ^{18}O EIE on outer-sphere electron transfer (~ 1.03) and the subsequent rate-limiting step. To account for ^{18}O KIEs $\ll 1.03$, a significant inverse ^{18}O KIE must characterize $O_2^{•-}$ binding to the oxidized metal.[17,20,21]

Another issue concerns the constraints of spin conservation. It has been reasoned that a concerted reaction where triplet O_2 reacts with a metal complex in the singlet state to afford a ground state singlet product is spin-forbidden and, therefore, should be kinetically disfavored. Sequential inner-sphere electron transfer involving a transient η^1-superoxide intermediate prior to rate-limiting η^1 to η^2 reorganization (eq 6) has been proposed to explain the rapid rates of reactions where η^2-peroxide complexes are formed from O_2.[55] Activation barriers for such reactions have been located by finding the minimum energy crossing points along the DFT calculated singlet and triplet surfaces.[69-71] The accurate

computation of the spin-state energies can be a complicating factor,[72] and additional problems derive from the difficulty in defining contributions from the activation entropy, i.e., identifying centrifugal barriers and the accompanying saddle-point structures.[73]

We have recently initiated DFT calculations to evaluate ^{18}O KIEs on irreversible O_2 coordination reactions within the context of Transition State Theory (TST). In accordance with TST, the ^{18}O KIE can be calculated from eq 11. This expression considers isotopic contributions from both the reaction coordinate frequency (ν_{RC}), the mode that converts a translation into a vibration at the transition state, and the pseudoequilibrium constant defined according to eq 12 for attaining the transition state from separated reactants (K_{TS}).

$$^{18}O \text{ KIE} = (^{16,16}\nu_{RC}/^{16,18}\nu_{RC})(^{16,16}K_{TS}/^{16,18}K_{TS}) \quad (11)$$

$$^{16,16}K_{TS}/^{16,18}K_{TS} = \text{ZPE} \times \text{EXC} \times \text{VP} \quad (12)$$

The expression for the isotope effect on K_{TS} resembles that of the ^{18}O EIE (eq 10), except the vibration corresponding to the reaction coordinate has been removed from the MMI partition function now referred to as the vibrational product (VP). When ν_{RC} is isotope independent, the ^{18}O KIE is fully determined by the isotope effect on K_{TS}. In this limiting case, the ^{18}O EIE is an upper limit to the ^{18}O KIE and the relationship ^{18}O KIE $< {}^{18}O$ EIE should hold as long as the transition state structure is intermediate of the reactant and product structures.

6. Implications of ^{18}O KIEs

A. Mechanisms of Metal-Mediated O_2 Activation. Measurements of ^{18}O KIEs on the irreversible formation of a number of η^2-peroxide compounds have been conducted and are summarized in Figure 4.[41,74] The reactions appear to exhibit ^{18}O KIEs that are less than the ^{18}O EIE$_{calc}$ or ^{18}O EIE$_{exp}$, although calculations involving the third-row transition metals have not yet been mastered.[46] Some of the results are further analyzed in Figure 5, where the ratio of the kinetic isotope effect to the equilibrium isotope effect (^{18}O KIE/^{18}O EIE) is taken as an indicator of the transition state structure. This parameter correlates to the second-order rate constants for O_2 binding (k_{O_2}) over a remarkable 7 orders of magnitude.

All of the reactions are thermodynamically downhill, with the increasingly favorable $\triangle G°$ believed to decrease $\triangle G^{\ddagger}$ and, consequently, increase k_{O_2}. Interestingly, the slowest reaction of O_2 with Ir^{I}Cl(CO)(PPh$_3$)$_2$ exhibits largest ^{18}O KIE/^{18}O EIE ~ 0.9. Yet a late transition state would seem difficult to justify in view of the favorable $\triangle G°(295$ K$) = -2.8$ kcal mol^{-1}.[43]

Until measurements become available in the endergonic regime, the question as to which theory best describes

(67) Taube, H. *Prog. Inorg. Chem.* **1986**, *34*, 607–625.

(68) Roth, J. P.; Klinman, J. P. *Proc. Natl. Acad. Sci. U.S.A.* **2003**, *100*, 62–67.

(69) Landis, C. R.; Morales, C. M.; Stahl, S. S. *J. Am. Chem. Soc.* **2004**, *126*, 16302–16303.

(70) Yu, H.; Fu, Y.; Guo, Q.; Lin, Z. *Organometallics* **2009**, *28*, 4443–4451.

(71) Strickland, N.; Harvey, J. N. *J. Phys. Chem. B* **2007**, *111*, 841–852.

(72) De la Lande, A.; Moliner, V.; Parisel, O. *J. Chem. Phys.* **2007**, *126*, 035102/1–035102/7.

(73) Aboelella, N. W.; Kryatov, S. V.; Gherman, B. F.; Brennessel, W. W.; Young, V. G., Jr.; Sarangi, R.; Rybak-Akimova, E. V.; Hodgson, K. O.; Hedman, B.; Solomon, E. I.; Cramer, C. J.; Tolman, W. B. *J. Am. Chem. Soc.* **2004**, *126*, 16896–16911.

(74) The half-life for O_2 binding to Cu^I(βDK) in DMF is estimated to be < 10 ms at 218 K on the basis of absorbance changes detected by rapid-mixing, stopped-flow spectrophotometry. The identity of the product under these conditions has been confirmed by ^{1}H NMR and resonance Raman spectroscopy. Roth, J. P.; Rybak-Akimova, E.; Tolman, W. B. Unpublished results.
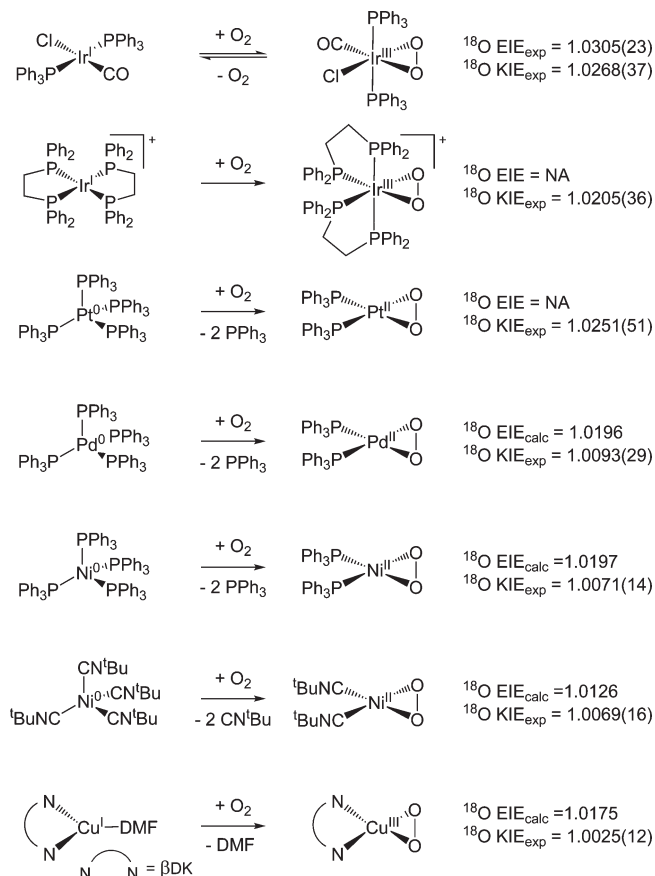
Figure 4. ^{18}O EIEs and ^{18}O KIEs determined at ambient and low temperature.[41,74]
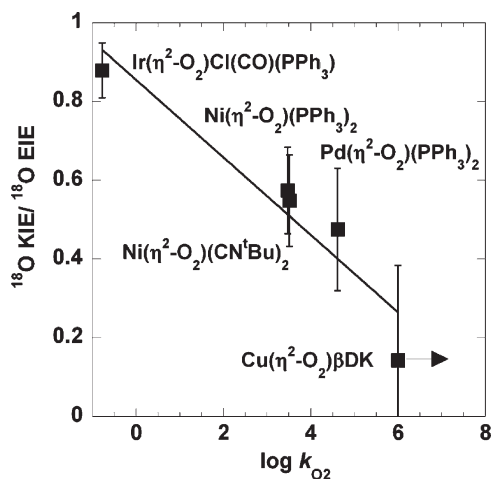

Figure 5. Variation of the transition state structure parameter (^{18}O KIE/^{18}O EIE) in response to the bimolecular rate constant for O_2 association (k_{O_2}).

the ^{18}O KIE to ^{18}O EIE relationship will remain open. As mentioned above, Marcus Theory[75] predicts that kinetic isotope effects should decrease as $\triangle G°$ deviates from thermoneutrality, while Hammond's postulate, on the basis of TST with an O–O stretching reaction coordinate, anticipates the maximum ^{18}O KIE as the reaction becomes increasingly unfavorable.
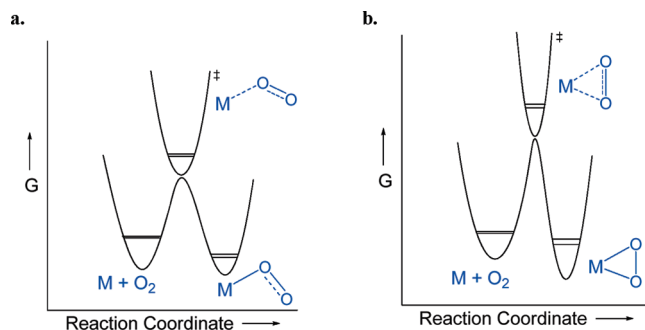
(75) Kresge, A. J. *J. Am. Chem. Soc.* **1980,** *102,* 7797–7798.

Figure 6. Single-step reactions resulting in the formation of η^1 and η^2 metal–O_2 adducts.

The correlation in Figure 5 is most readily attributable to single-step, inner-sphere electron transfer, contrary to the predictions of some recent DFT computational studies.[55,70] Figure 6 depicts this associative mechanism for η^1-superoxide and η^2-peroxide complexes. In the reaction coordinate diagrams, the position of the transition state is expected to vary smoothly with the driving force of the rate-determining step. To be consistent with the trend in Figure 5, all reactions should have similar intrinsic barriers, i.e., the $\lambda/4$ term in Marcus Theory reflecting reorganization of intramolecular bond lengths and angles as well as the solvent. When the isotope effect on the reaction coordinate frequency is negligible, the ^{18}O KIE may derive mostly from the isotopically sensitive λ. The ^{18}O EIE could dictate the limit of the isotope effect on λ, with values falling into different ranges for the η^1-superoxide (<1.015) and η^2-peroxide ($1.020-1.030$) structures. In addition to the magnitude of the ^{18}O KIE, the correlation of ^{18}O KIE/^{18}O EIE to k_{O_2} is also a distinguishing factor arising from the differences in λ.

As mentioned above, sequential inner-sphere electron transfer has been proposed as an alternative to the concerted mechanism for η^2-peroxide formation shown in Figure 6b.[55,70] A wide range of ^{18}O KIEs, from 1.0069(16) to 1.0268(37), has been determined for such reactions (Figure 4), with no intermediate being detectable in any case.[16,41,73,74] The size of the ^{18}O KIEs on the reactions in Figure 7 would be expected to differ depending upon whether the first or second transition state is the highest point along the reaction coordinate. If the η^1-superoxide intermediate were formed irreversibly in the initial O_2 association step (Figure 7a), the ^{18}O KIE could be smaller than the accompanying ^{18}O EIE. This is clearly not the case for η^2-peroxide-forming reactions, where ^{18}O KIEs are between 1.0205(36) and 1.0268(37) cf. Figure 4.[41] A different scenario is shown in Figure 7b, where the second step is rate-limiting. The observed ^{18}O KIE is expected to be larger than the ^{18}O EIE for η^1-superoxide formation and smaller than the ^{18}O EIE expected for η^2-peroxide formation. Most experimental data appear to be inconsistent with these limits, although ^{18}O EIEs have yet to be determined for some of the late-transition-metal η^1-superoxide structures.

It can be difficult to exclude the formation of an η^1-superoxide intermediate when this species is significantly higher in energy than the separated reactants. Such a mechanism is, however, unlikely in view of the
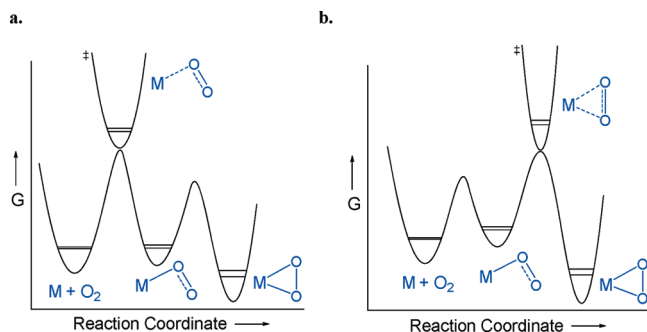
a.
b.

Figure 7. Alternate sequential mechanisms for the formation of the η^2 metal$-O_2$ adduct.

correlation been ^{18}O KIE/^{18}O EIE and k_{O_2} for η^2-peroxide formation. The increase in k_{O_2} and concomitant decrease in ^{18}O KIE/^{18}O EIE are attributed to $\triangle G°$ becoming more favorable. In the mechanism where the second step is rate-determining, $\triangle G^{\ddagger}$ can be lowered by stabilizing the product or destabilizing the η^1-superoxide intermediate. Because destabilization of the intermediate also raises the barrier to its formation, at some point over the several orders of magnitude variation in k_{O_2}, the rate-limiting step would be expected to change from $\eta^1 \rightarrow \eta^2$ reorganization (Figure 7b) to rate-limiting O_2 association (Figure 7a).

The absence of spectrophotometrically detectable intermediates further argues against the two-step mechanism for forming η^2-peroxide complexes. Calculations by Stahl, Landis, and co-workers[55] have slightly favored the sequential inner-sphere mechanism over concerted two-electron transfer for reactions of Pd^0 complexes with O_2 reaction. The former would involve a $Pd^I(\eta^1-O_2^{I-})$ intermediate predicted to be enthalpically stabilized relative to the reactants by -7.5 kcal mol^{-1}. Accounting for the reaction entropy would result in $\triangle G°_{298 K} \sim 0.7$ kcal mol^{-1}. The energetics suggests that accumulation of the η^1-superoxide intermediate prior to the rate-limiting step could be observed at sufficiently high O_2 concentrations or at low temperatures.

B. Superoxide Oxidation: Examining O_2 Activation in Reverse? The mechanism of metal-mediated $O_2^{\bullet-}$ oxidation has been examined in an effort to evaluate the possibility of preequilibrium outer-sphere electron transfer during O_2 reductive activation (eq 5). Studies of ^{18}O KIEs have been conducted on the reactions of copper(II) tris(pyridylamine) complexes with KO_2 in polar organic solvents. These rapid reactions have been proposed to form $[Cu^{II}(\eta^1-O_2)(TEPA)]^+$ and $[Cu^{II}(\eta^1-O_2)(TMPA)]^+$ (cf. Figure 2) as intermediates prior to the release of O_2.[21]

Rapid-mixing stopped-flow studies at 193 K[21] provided further evidence of $[Cu^{II}(\eta^1-O_2)(TMPA)]^+$. The optical absorbance spectrum was identical with that observed upon oxygenation of $[Cu^I(TMPA)]^+$ under the same experimental conditions and similar to that reported in earlier studies.[76] The absorbance spectrum resembles the crystallographically characterized $[Cu(\eta^1-O_2)TMG_3tren]^+$, generated upon reacting O_2 with
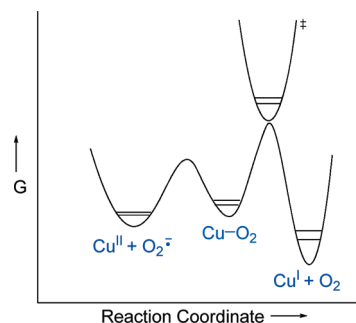

Figure 8. Proposed mechanism of $O_2^{\bullet-}$ oxidation by copper(II) tris-(pyridylamine) complexes.

$[Cu^I(TMG_3tren)]^+$ at low temperature[44,77] and differs from those reported for copper-derived η^2-superoxide/peroxide complexes.[63] Similar to the results for transition-metal complexes from groups VIII$-$X, the measured and calculated ^{18}O EIEs associated with the $Cu(\eta^1-O_2)$ and $Cu(\eta^2-O_2)$ structures also fall within discernibly different ranges.

The Cu^{II} complexes have been proposed to react with $O_2^{\bullet-}$ by a sequential mechanism involving a $Cu-O_2$ intermediate rather than direct, outer-sphere electron transfer (Figure 8). This conclusion was reached largely on the basis of the inverse ^{18}O KIEs observed to fall within a relatively narrow range of $0.984(6)-0.989(8)$ in spite of the large variation in the effective $\triangle G°$ from -6 to -19 kcal mol^{-1}.[21] In addition, the ^{18}O KIEs are independent of whether an additional coordinating ligand (N_3^-) is present. The presence of N_3^- would be expected to influence the barrier to $O_2^{\bullet-}$ oxidation.

The observation of inverse ^{18}O KIEs which are insensitive to large changes in $\triangle G°$ suggests that bonding changes occur in a preequilibrium step. This proposal also explains the insensitivity to the change in the complex coordination geometry. ^{18}O KIEs between 1 and the limiting ^{18}O EIE$_{calc}$ of 0.968 for $O_2^{\bullet-}$ oxidation to O_2 are expected for the reversible binding of $O_2^{\bullet-}$ to Cu^{II}, followed by dissociation of O_2 in the rate-limiting step. Resemblance of the intermediate and transition state to the $Cu-O_2$ structures in Figure 2 has been attributed to the very favorable thermodynamics of the second step.[21]

Isotopic measurements have also provided evidence of $Cu-O_2$ intermediates in enzymatic reactions of $O_2^{\bullet-}$. An inverse ^{18}O KIE $= 0.9722(16)$ was determined for $O_2^{\bullet-}$ oxidation by $Cu^{II}Zn$ superoxide dismutase (SOD).[20] The mechanism of SOD appears to be similar to that of the synthetic copper(II) complexes, although the ^{18}O KIE implicates a more $Cu^I-O_2^0$-like transition state. In support of this proposal, the nonenzymatic reaction of O_2 with Cu^IZnSOD exhibits an ^{18}O KIE $= 1.0044(16)$. This small effect is consistent with an inner-sphere pathway and incompatible with the larger ^{18}O KIEs, from 1.025 to 1.030, that characterize outer-sphere electron transfers.[68,78]

The electrostatically bound $Cu-O_2$ intermediate apparently forms via an $O_2^{\bullet-}$ association barrier that is lower than that of the redox reaction facilitating the release of O_2. The latter requires intramolecular bond reorganization and changes in the coordination geometry about the

(76) Zhang, C. X.; Kaderli, S.; Costas, M.; Kim, E.-I.; Neuhold, Y.-M.; Karlin, K. D.; Zuberbuhler, A. D. *Inorg. Chem.* **2003**, *42*, 1807–1824.

(77) Wuertele, C.; Gaoutchenova, E.; Harms, K.; Holthausen, M. C.; Sundermeyer, J.; Schindler, S. *Angew. Chem., Int. Ed.* **2006**, *45*, 3867–3869.

(78) Roth, J. P.; Wincek, R.; Nodet, G.; Edmondson, D. E.; McIntire, W. S.; Klinman, J. P. *J. Am. Chem. Soc.* **2004**, *126*, 15120–15131.

metal. Considering the microscopic reverse of $O_2^{\bullet-}$ oxidation by Cu^{II}, from right to left in Figure 8, O_2 reduction is thermodynamically unfavorable and likely involves formation of a $Cu(\eta^1\text{-}O_2)$ intermediate in the rate-limiting step. This proposal is in direct contrast to the sequential outer-sphere electron transfer mechanism in eq 5, where $O_2^{\bullet-}$ forms before binding to the oxidized metal cofactor.[32,33]

7. O−O Bond Rupture and the Microscopic Reverse: O−O Bond Formation

Combined experimental and computational studies have recently been applied to analyze oxygen isotope effects on the activation of H_2O_2 and thereby elucidate the mechanism of heme peroxidases. Significantly, these studies have drawn attention to the isotope sensitivity of the reaction coordinate previously proposed to be an important contributor to heavy-atom kinetic isotope effects.[30] Recent DFT studies have not, addressed this issue, although it is likely to be important for metal-mediated small-molecule activation reactions that result in bond cleavage.[56,67,69−71,79−81]

In horseradish peroxidase (HRP), the enzyme's prosthetic group, $Fe^{III}(Por)$ (Por = protoporphyrin IX), reacts with H_2O_2 to produce $Fe^{IV}O(Por^{\bullet+})$ and H_2O. Largely on the basis of intuition concerning the stability of the products, Poulos and Kraut proposed a single-step O−O heterolysis mechanism.[82] During catalysis, exogenous reductants react with the $Fe^{IV}O(Por^{\bullet+})$ as well as the subsequently formed $Fe^{IV}O(Por)$ to regenerate $Fe^{III}HRP$.

HRP has now been examined in greater depth using oxygen isotope fractionation as a mechanistic probe of H_2O_2 activation during enzyme turnover.[23] The reaction of $Fe^{III}HRP$ with H_2O_2 in the presence of the reducing agent 2-methoxyphenol is characterized by an ^{18}O KIE = 1.0127 ± 0.0008. This value is slightly larger than the theoretical ^{18}O EIE_{calc} = 1.0105 for O−O heterolysis but much smaller than the ^{18}O EIE_{calc} = 1.0300 for O−O homolysis, which could produce $Fe^{IV}O(Por)$ and $^{\bullet}OH$ prior to $Fe^{IV}O(Por^{\bullet+})$ and H_2O. That the ^{18}O KIE is much less than the latter ^{18}O EIE_{calc} excludes homolysis as a reversible, preequilibrium step.

DFT calculations were performed to find the transition states associated with the one- and two-electron O−O bond cleavage reactions. The starting point was a higher energy $Fe^{III}OOH(Por)$ intermediate hydrogen-bonded through the β-O to a distal imidazole side chain.[83] The transition state for homolysis could not be located, consistent with a prohibitively high energy pathway. In contrast, the transition state for heterolysis was found to be slightly higher in energy than the hydrogen-bonded intermediate (E_a = +2.4 kcal mol^{-1}). This transition state, designated as #2 in Figure 9, is situated above the barrier preceding the rate-limiting step.

Transition state vibrational frequencies and imaginary modes for each isotopologue were used to compute the ^{18}O
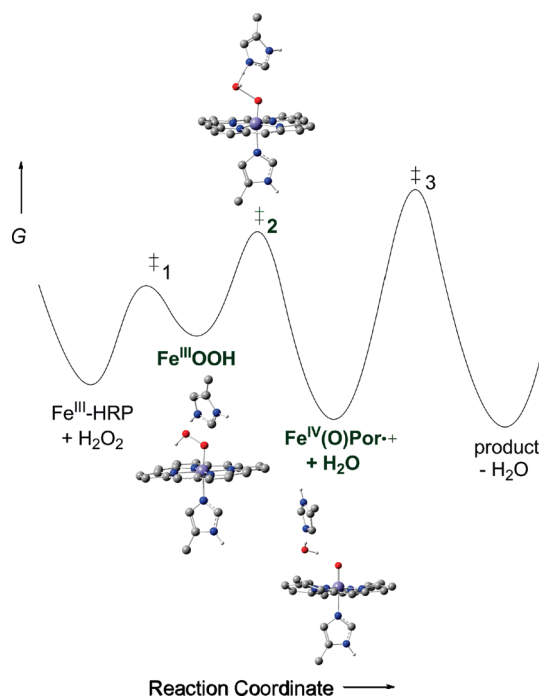

Figure 9. Proposed mechanism of reversible O−O heterolysis in HRP.

KIE for O−O heterolysis. A theoretical ^{18}O KIE_{calc} = 1.0320 significantly exceeding the ^{18}O EIE_{calc} = 1.0105 was derived from isotope-dependent ν_{RC} and K_{TS} terms in eq 11. The isotope effect on the reaction coordinate frequency, $^{18}\nu_{RC}$ = 1.020, arises from imaginary frequencies of 226.5i and 222.0i cm^{-1} for the light and heavy isotopologues. The calculation involved statistical averaging of the 224.1i cm^{-1} mode associated with $Fe\text{−}^{16}O\text{−}^{18}O\text{−}H$ and the 220.0i cm^{-1} mode associated with $Fe\text{−}^{18}O\text{−}^{16}O\text{−}H$, as previously described.[42] The isotope effect on the pseudoequilibrium constant, $^{18}K_{TS}$ = 1.0117, was calculated similarly using only the stable vibrations.

Disagreement between the ^{18}O KIE_{calc} = 1.0320 and the measured ^{18}O KIE of 1.0127 suggests that O−O cleavage is not rate-limiting. Instead, O−O heterolysis is proposed to be a preequilibrium step before a weakly isotope-sensitive ferryl reduction or protein conformational change. The reversible second step in Figure 9 is consistent with the computed ΔG° = −4.9 kcal mol^{-1} as well as the lower limit of ^{18}O EIE_{calc} = 1.0105 for O−O heterolysis.

More compelling evidence for reversible O−O bond breaking/making during HRP catalysis comes from tracer experiments in conjunction with measurements of the H_2O_2 isotope fractionation. The reaction in 1.2% ^{18}O-labeled water revealed a striking increase in the $^{18}O/^{16}O$ of the unreacted H_2O_2 relative to its composition in natural abundance water as the reaction progressed. Thus, the ^{18}O KIE was dramatically altered in a manner consistent with rapid exchange of the ^{18}O label from H_2O into the unreacted H_2O_2 on the time scale of the peroxidase reaction.

The reversible O−O bond making/breaking proposed for HRP has little precedent in the literature,[84,85] although there

(79) Slaughter, L. M.; Wolczanski, P. T.; Klinckman, T. R.; Cundari, T. R. *J. Am. Chem. Soc.* **2000**, *122*, 7953−7975.

(80) Abu-Hasanayn, F.; Goldman, A. S.; Krogh-Jespersen, K. *J. Phys. Chem.* **1993**, *97*, 5890−5896.

(81) Nowlan, D. T.; Gregg, T. M.; Davies, H. M. L.; Singleton, D. A. *J. Am. Chem. Soc.* **2003**, *125*, 15902−15911.

(82) Poulos, T. L.; Kraut, J. *J. Biol. Chem.* **1980**, *255*, 8199−8205.

(83) Zazza, C.; Amadei, A.; Palma, A.; Sanna, N.; Tatoli, S.; Aschi, M. *J. Phys. Chem. B* **2008**, *112*, 3184−3192.

(84) Marquez, L. A.; Huang, J. T.; Dunford, H. B. *Biochemistry* **1994**, *33*, 1447−1454.

(85) Halfen, J. A.; Mahapatra, S.; Wilkinson, E. C.; Kaderli, S.; Young, V. G., Jr.; Que, L., Jr.; Zuberbuehler, A. D.; Tolman, W. B. *Science* **1996**, *271*, 1397−1400.

are examples of related reactions involving nucleophilic attack upon electrophilic metal−oxo species.[86−88] Such mechanisms are commonly accepted for halide oxidation by mammalian heme peroxidases.[89] Isotope fractionation studies of HRP are unique in providing evidence of reversible O−O bond formation/cleavage by a two-electron pathway.

Findings from the studies of H_2O_2 activation raise new questions concerning the isotope sensitivity of reaction coordinates and the implications this has on the boundary conditions used to interpret [18]O KIEs. There are a few studies which have assumed that [18]O EIEs provide upper limits to [18]O KIEs regardless of the reaction mechanism.[25,56,90] The [18]O KIEs reported in the cited works are associated with the formation of an iron(IV) oxo species from O_2. The mechanistic interpretations may need to be revised pending experimental studies that address the relationship of [18]O KIEs to [18]O EIEs on defined reactions where O_2 activation progresses to the level of O−O bond breaking.

8. Future Directions: Isotopic Studies of Water Oxidation

Several years ago, Babcock et al.[91] proposed that O−O bond cleavage by heme peroxidases could be thought of as the microscopic reverse of O−O bond formation. Therefore, O−O heterolysis could be related to the nucleophilic attack of water or hydroxide upon an electrophilic metal−oxo species, as proposed for the reactive manganyl ($Mn^V=O$) in the oxygen-evolving complex of photosystem II (PSII; Figure 10).

Though the Kok cycle in Figure 10 has been the subject of numerous biochemical, biophysical, and biomimetic studies, the mechanism of O−O formation within the O_2-evolving complex remains obscure. Evidence for a manganese-bound intermediate with an O−O bond intact has recently been obtained from kinetic studies at high pressures of O_2.[92] This result suggests that S_0 and S_4 might interconvert via an intermediate designated as S_4' in a kinetically accessible equilibrium.

Competitive oxygen isotope fractionation has been applied to study the O_2 evolved during photosynthesis[93] using an apparatus that is the prototype for the one described in this review. Though only a slight difference in the oxygen isotope composition from natural abundance H_2O was detectable, follow-up studies performed using different experimental strategies have uncovered significantly inverse [18]O KIE.[94,95] The reason for the
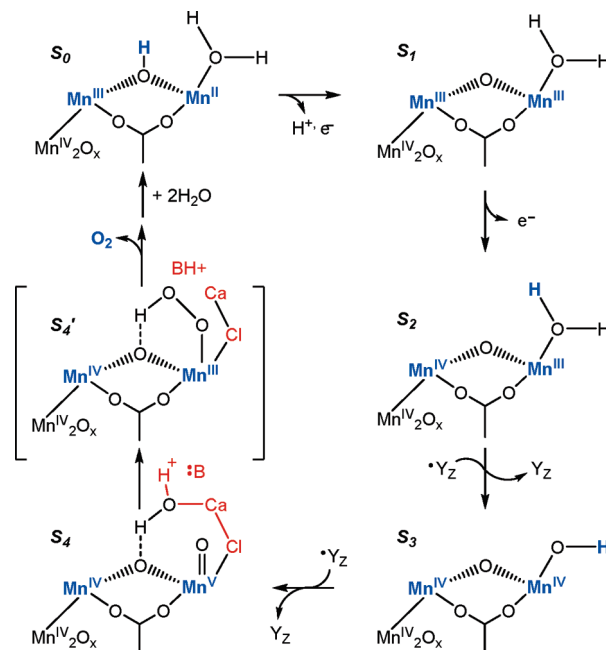

Figure 10. Reactions proposed to accompany photonic $S_0 \rightarrow S_4$ transitions in PSII.

inconsistent results has remained unresolved in part because of the absence of benchmarks and uncertainties regarding theoretical interpretations.[96]

We have begun to apply oxygen isotope fractionation to study reactions of synthetic inorganic compounds proposed to effect water oxidation via high-valent metal−oxo species. The goal is to use competitive [18]O KIEs to differentiate mechanisms of O−O bond formation that involve intramolecular radical coupling from those involving nucleophilic attack. Models for one- and two-electron transfer reactions will provide a much needed framework for illuminating the mechanism of PSII and may facilitate the design of new synthetic catalysts capable of photochemical water oxidation.

Structurally characterized manganese, ruthenium, and iridium complexes,[97] proposed to mediate O−O bond formation, will be systematically investigated. The steps involving H_2O activation and release of O_2 will be addressed. Measurements of competitive [18]O KIEs are being performed in conjunction with DFT calculations. In light of the results obtained from studies of peroxidase reactivity,[23] significant differences in the magnitudes of [18]O KIEs and [18]O EIEs are anticipated for O−O bond formation by one- electron and two-electron pathways.

Future studies of O−O bond activation during water oxidation will complement our understanding of metal-mediated O_2 reductive activation. Although much progress has been made by examining reactions of structurally defined inorganic molecules, physical insights as to the origins of oxygen isotope effects on specific types of reactions, e.g., O−O homolysis and heterolysis, are still needed. In the end, the marriage of theory and experiment will be required to establish mechanisms of small-molecule activation and

(86) Furutachi, H.; Hashimoto, K.; Nagatomo, S.; Endo, T.; Fujinama, S.; Watanabe, Y.; Kitagawa, T.; Suzuki, M. *J. Am. Chem. Soc.* **2005**, *127*, 4550–4552.

(87) Jin, N.; Bourassa, J. L.; Tizio, S. C.; Groves, J. T. *Angew. Chem., Int. Ed.* **2000**, *39*, 3849–3851.

(88) Nam, W.; Choi, S. K.; Lim, M. H.; Rohde, J.-U.; Kim, I.; Kim, J.; Kim, C.; Que, L. *Angew. Chem., Int. Ed.* **2003**, *42*, 109–111.

(89) *Peroxidases in Chemistry and Biology*; Everse, J., Everse, K. E., Grisham, M. B., Eds.; CRC Press: Boca Raton, FL, 1991; Vol. *1*.

(90) Mirica, L. M.; Klinman, J. P. *Proc. Natl. Acad. Sci. U.S.A.* **2008**, *105*, 1814–1819.

(91) Hoganson, C. W.; Pressler, M. A.; Proshlyakov, D. A.; Babcock, G. T. *Biochim. Biophys. Acta, Bioenerg.* **1998**, *1365*, 170–174.

(92) Clausen, J.; Junge, W. *Nature* **2004**, *430*, 480–483.

(93) Guy, R. D.; Fogel, M. L.; Berry, J. A. *Plant Phys.* **1993**, *101*, 37–47.

(94) Metzner, H.; Fischer, K.; Bazlen, O. *Biochim. Biophys. Acta* **1979**, *548*, 287–295.

(95) Burda, K.; Bader, K. P.; Schmid, G. H. *Biochim. Biophys. Acta, Bioenerg.* **2003**, *1557*, 77–82.

(96) Tcherkez, G.; Farquhuar, G. D. *Funct. Plant Biol.* **2007**, *34*, 1049–1052.

(97) Eisenberg, R.; Gray, H. B. *Inorg. Chem.* **2008**, *47*, 1697−1699 and references cited therein.

parlay our predictive understanding into the production of clean fuels and commodity chemicals.